Optical Pumping of Rubidium

Joe Blake, Will Bolton, and Michael Negus

(Dated: 23 December 2022)

An investigation into the atomic properties of rubidium. This includes calculating the nuclear spins of ^{87}Rb & ^{85}Rb and observing the quadratic Zeeman effect and transient effects.

I. INTRODUCTION

Optical pumping is a method of using photons to excite electrons in atoms in a target material so emission spectra can be observed; the input photon frequency chosen depends on the electronic ground state transitions of the target atoms. It is used in lasers to raise electron energy level to a metastable state[1] and for experimentally measuring hyperfine structure of atoms[2].

Developed in the early 1950s by Alfred Kastler, it subsequently won him a Nobel Prize in 1966 for "The discovery and development of optical methods for studying Hertzian resonances in atoms"[3]. In our experiment we will use optical pumping to measure various atomic properties of rubidium, including the nuclear spin, and will attempt to observe the quadratic Zeeman effect and transient effects.

II. THEORY[4]

The ground state of alkali atoms consists of several closed shells and one valence electron in the outermost shell. Rubidium can be described by the noble gas configuration, Rb: [Kr] 5s.[5]

By spherical symmetry, the momentum of each closed shell is zero. This means that the total angular momentum is the sum of the orbital and spin angular momenta of the valence electron and the nuclear angular momentum.

We denote the electron's orbital angular momentum **L** and its spin angular momentum **S** which sum to its total non-nuclear angular momentum, **J**. Each component of angular momentum has an associated magnetic dipole moment μ_L and μ_S. Since our investigation is concerned only with the hyperfine structure of the ground state, we neglect the effects of spin-orbit coupling, setting value of **L** to be zero. This means the total angular momentum will have the value: J = S = $\hbar/2$. In the first excited state, L = $\hbar$. This means J can now be either L + S or L - S giving a total of two possible states which the valence electron could occupy; these two states have differing energies and this difference determines the fine structure. In general, each excited state is split into ℓ levels of degeneracy where ℓ is the orbital quantum number.

Further splitting of the energy levels known as hyperfine structure must also be considered. Hyperfine structure originates from the coupling of nuclear magnetic dipole moments (from nuclear spin) and the electronic magnetic dipole moment associated with **J**, forming a total atomic angular momentum **F**, which is the sum of **J** and the nuclear spin component, **I**.

When an external magnetic field is applied we can observe the Zeeman effect. This splitting of energy levels is very small compared to hyperfine splitting for weak magnetic fields. It arises form interaction between the external magnetic field and the magnetic dipole moment associated with the orbital angular momentum and splits each F-state (from the hyperfine splitting) into $2\ell+1$ energy levels.

In the calculation of the first order energy perturbation of an atom in a weak magnetic field, a multiplicative constant arises. It relates the total magnetic energy to the strength of the applied field and the component of the electron spin along the magnetic field, and is known as the Landé g-factor.

$$\text{Magnetic Energy} = g_F \mu_0 M B$$

First, consider only the fine splitting. Using the vector model outlined above this can be determined to be:

$$g_J = 1 + \frac{J(J+1) + S(S+1) - L(L+1)}{2J(J+1)}$$

Including nuclear effects we have:

$$g_F = g_J \frac{F(F+1) + J(J+1) - I(I+1)}{2F(F+1)} \tag{1}$$

In the ground state we have L = 0, S = J = $\frac{1}{2}$. This gives:

$$g_J = 1 + \frac{\frac{1}{2}(\frac{1}{2}+1) + \frac{1}{2}(\frac{1}{2}+1) - 0(1)}{2(\frac{1}{2})(\frac{1}{2}+1)} = 2 \tag{2}$$

Using perturbation theory leads to the Breit-Rabi equation which gives energy as a function of the total angular momentum and the component of the electron spin along the magnetic field. It shows that when the magnetic field is close to zero, the energy levels split linearly with field strength. There is then a quadratic dependence as the field increases which corresponds the the decoupling of I and J before the dependence becomes linear again.

III. METHODS

The photon source is a sample of two rubidium isotopes in the ratio of their natural relative abundance, 72% ^{85}Rb and 28% ^{87}Rb. These isotopes are vaporised inside a bulb with an inert gas buffer of xenon. In addition to being chemically inert, xenon is electronically spherically symmetric, meaning collisions with xenon will not affect the angular momentum of the rubidium ions.

Around the bulb are wire coils whose current varies sinusoidally. The magnetic field induced by the coil interacts with the vaporised rubidium ions, increasing their kinetic energy. Collisions cause the rubidium ions to enter excited electronic states. When these electrons fall back to their ground state, photons are emitted with frequencies corresponding to energy level differences.

After emission, the light passes through a plano-convex lens, designed to focus light rays towards the a central point where the rubidium sample will be placed. The light passes through an interference filter and a linear polariser to ensure subsequent homogeneity, and then through a quarter wave plate to be circularly polarised.

The light then passes into the rubidium vapour absorption cell which is housed within an oven heated to 50°C. The cell is

surrounded by two pairs of Helmholtz coils aligned in the x-y and x-z planes (assuming photon emission in the $+z$ direction). The absorption cell has a buffer gas of 30 torr neon, used for the same reasons as the xenon in the bulb. The Helmholtz coils are used to create pseudo-uniform magnetic fields and both pairs are oriented to be centred around the rubidium sample. This creates a constant magnetic field throughout the sample. A DC current passing through these coils is tuned to cancel out the Earth's magnetic field at the sample.

We also have horizontal sweep coils, which are used to precisely change magnetic field in search of resonances. These main coils are all managed by the TEACHSPIN Optical Pumping OPI-D OPI-B device[6]. Perpendicular to both other coils (now in the y-z plane) are the RF coils, situated directly outside the sample container. This pair do not satisfy the Helmholtz condition, but instead are connected to an RF function generator and are used provide energy and induce transitions between states in the rubidium sample. To create different amplitudes, frequencies and waveforms, a dedicated RF function generator is used.

After passing through the sample, the light is recollimated by another plano-convex lens. The detector is a silicon photodiode from Photonic Detectors Inc. PDB-C108[8]. The gain on the detector is high, so it is cathode grounded in an attempt to minimise noise. The entire equipment set is then covered in a thick black shroud to minimise the amount of external light received by the detector.

The detector is connected to a Tektronix TDS 2024B Digital Storage Oscilloscope[9], which is used to view and compare the many signals involved.

IV. EXPERIMENTS

A. Low field determination of nuclear spins

The absorption cell has two isotopes of rubidium, ^{85}Rb and ^{87}Rb, each with different values of nuclear spin. In order to calculate these spins, the g-factor for an atom with total atomic angular momentum, g_F, must be measured for each isotope. To calculate g_F, we measured a resonant frequency of each isotope at various values of the applied magnetic field from the RF coils.

The value of the magnetic field was determined approximately using the geometry of the coils and the magnitude of the applied current. This approximation was justified as the nuclear spins are either integral or half integral, so the precision of observations was inconsequential when well within the half-integer range. The magnetic field can be calculated using:

$$B = \left(\frac{4}{5}\right)^{3/2} \frac{\mu_0 I N}{R} \tag{3}$$

where μ_0 is the permeability of free space, I is the current through the sweep coils, N is the number of turns of wire in each of the coils and R is the mean radius of the coils. For our equipment, $R = 0.1639$ m, $N = 11$ and $\mu_0 = 1.2566 \times 10^{-6}$ m kg s^{-2}A^{-2}. Using these, equation (3) gives:

$$B = \alpha I \tag{4}$$

with B measured in Tesla (T), I measured in amps (A) and $\alpha = 6.035 \times 10^{-5}$T/A.

First, the residual field due to the Earth's magnetic field at the absorption cell was determined; this was done by disconnecting the main coils to isolate the sweep field. The sweep coils were then adjusted to find the zero-field resonance dip. Notably this required the equipment to be oriented antiparallel to the Earth's magnetic field lines. The current at this resonance was recorded and equation (4) used to calculate the residual field. The value of current through the sweep coils at this point was taken from future recordings in order to calibrate.

To find different Zeeman resonances a sinusoidal signal was generated in the RF coils, and at varying frequencies the horizontal magnetic field was swept until dips were observed. These observations were made in a frequency range of 30kHz up to 350kHz, and three resonance dips were found at each frequency. The largest of these corresponded to the zero-field transmission, whose magnitude was a result of both isotopes contributing additively, so was ignored. The other two dips corresponded to resonances from each isotope of rubidium. The current at each resonance was recorded, and equation (4) used to calculate the corresponding magnetic field in the RF coils. For each dip, the increasing frequency was plotted against magnetic field. By calculating the line of best fit for these plots, a numerical value a for the linear relationship between frequency f and magnetic field strength B was found, such that $B = af$. The theoretical equation relating the frequency and magnetic field is the resonance equation:

$$B = \frac{h}{g_F \mu_B} f \tag{5}$$

where h is Planck's constant and μ_B is the Bohr magneton.

Substituting a into the resonance equation gives:

$$g_F = \frac{h}{a \mu_B} \tag{6}$$

The theoretical relation between the quantum numbers F, J and I, the Landé g factor, g_J and g_F is given in equation (1). (1) was then solved for the nuclear spin, I, for each isotope.

B. Sweep field calibration

For the rest of the experiments a more precise value of the magnetic field was required as opposed to the approximation of equation (4). The sweep field were calibrated using the known g_F values that were calculated in the previous experiment.

The magnetic field strength can be calculated using the resonance equation (5).

For a range of resonant frequencies of each isotope, this equation was then used used to calculate the magnetic field strength, as g_F was known from IV A. The magnetic field strength was then plotted against current for each isotope. As a check, these plots should have been nearly identical, as the sweep coil magnetic field is independent of the rubidium. A line of best fit of these plots gave the magnetic field as a linear function of current in the sweep coils. As before, the value for the residual magnetic field was taken away from the results.

C. Main field calibration

Calibration for the magnetic field due to the main coils was also required. A method similar to the calibration of the sweep

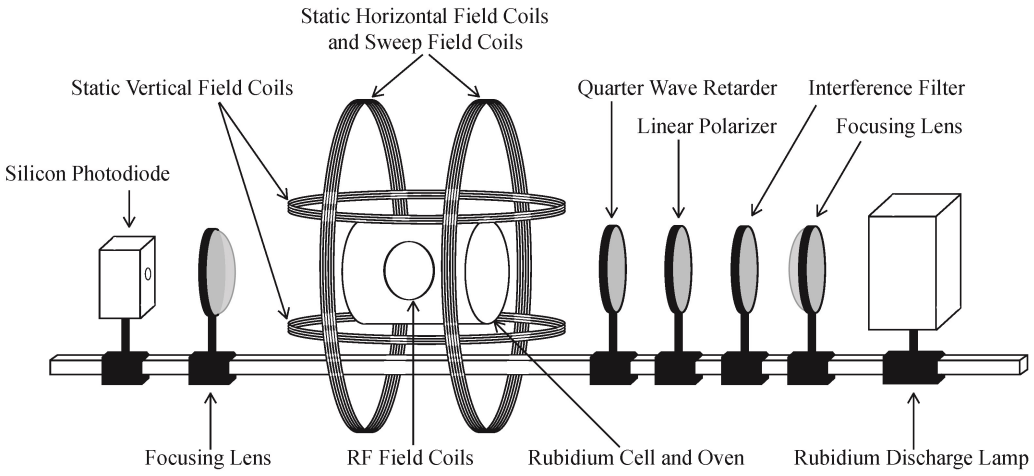

FIG. 1. A diagram of the experimental equipment setup[7]

coils was used, however the main coils are too coarse to allow the resonances to be centred well using it alone. Hence, both the sweep and the main coils were used to find resonances. The total magnetic field strength then had three components:

$$B_{\text{total}} = B_{\text{sweep}} + B_{\text{main}} + B_{\text{residue}} \tag{7}$$

This scalar equation is justified as all three fields are colinear. Plugging B_{total} into the resonance equation 5 gives:

$$B_{\text{main}} = \frac{h}{g_F \mu_B} f - B_{\text{sweep}} - B_{\text{residue}} \tag{8}$$

The experiment then involved adjusting the current in the sweep and main coils at varying frequencies to find resonance dips for each isotope of rubidium. As the formula for B_{sweep} was calculated in the sweep field calibration, and g_F for each isotope known, a formula for B_{main} as a function of the current in the main coils results from using the line of best fit of B_{main} against I_{main}.

D. Quadratic Zeeman effect

In the previous experiments, the magnetic field strength, B, was low, where the energy level splitting was linear with respect to B. This becomes non-linear as B increases. Each zero-field energy level splits into $2F+1$ sublevels thus in this region there are $2F$ resonances whose splitting can be resolved. For ^{87}Rb, where the nuclear spin $I = \frac{3}{2}$, there are a total of six resonances due to the allowed transitions $\Delta F = 0$ and $\Delta M = \pm 1$. Similarly, for ^{85}Rb, where $I = \frac{5}{2}$, there are a total of ten.

As before, the resonance equation (5) can be used to determine the magnetic field needed to observe resonances at different frequencies of RF for a particular isotope. In the experiment, we started with no current in the main field coils, and used the sweep coils to centre on the zero-field transmission, as in section IV A. The current in the main coils were then set such that the magnetic field is the desired value from the resonance equation, using the main field calibration from section IV C. The sweep field was then used to observe all of the resonances from the Zeeman splitting.

E. Transient effects

This experiment was to observe transient effects by centring into a low field resonance and switching the RF on and off by means of a square wave pulse.

The frequency of the square wave was set to 4Hz, and the amplitude was varied. When the RF is on, no optical pumping takes place and the transmitted light intensity is minimum. Turning off the RF allows optical pumping to begin and the transmitted light intensity increases $\sim e^{-t}$ converging to a maximum value. When the RF is turned on again, transitions occur between the Zeeman sublevels and the population of the sublevels converges toward equilibrium. This results in damped oscillations of the transmitted light, eventually levelling out to the minimum at the start, and then the process repeats.

The time period of the damped oscillations at different amplitudes of RF was measured in order to obtain a numerical relation. Theoretically, the time period should be inversely proportional to amplitude[4].

V. RESULTS

A. Low field determination of nuclear spins

As expected, three resonance dips were observed through sweeping the magnetic field, as show in FIG. 2.

The first dip is the large zero-field resonance. The other two dips are due to the individual rubidium isotopes. The residual field at the absorption cell was found to be 1.56×10^{-5}T, and the magnetic fields for the Zeeman resonances were calculated and plotted in FIG. 3. The slopes for these two plots are $a_1 = (1.40 \pm 0.05) \times 10^{-10}$T/Hz and $a_2 = (2.09 \pm 0.05) \times 10^{-10}$T/Hz. Using equation (6), the experimental values for g_F were found

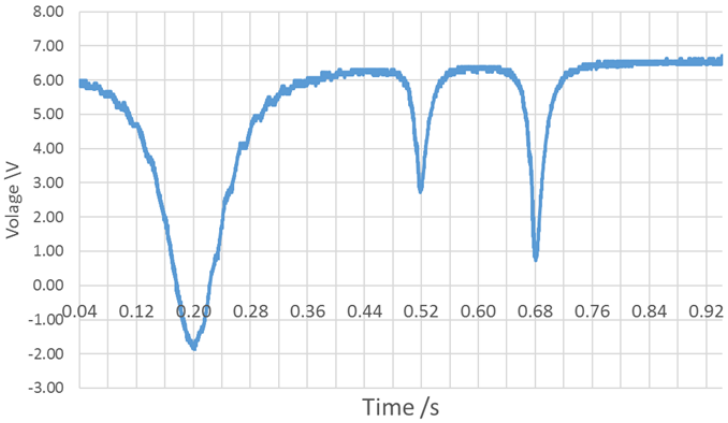

FIG. 2. Three resonance dips corresponding to absorption. The first is the zero-field dip due to both isotopes. The other two are due to single isotopes.

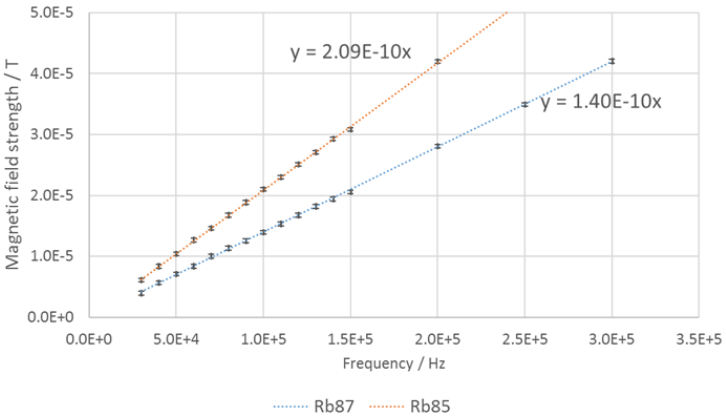

FIG. 3. Magnetic field strength vs. Frequency for the two isotopes of rubidium. Note: The error bars are small so are barely visible

to be $g_F^1 = 0.51 \pm 0.018$ for the first non-zero-field resonance dip, and $g_F^2 = 0.34 \pm 0.008$ for the second.

The theoretical values are $g_F = \frac{1}{2}$ for ^{87}Rb and $g_F = \frac{1}{3}$ for ^{87}Rb, so we can conclude from the calculated g_F values, that the first non-zero-field dip was due to ^{87}Rb and the other was due to ^{85}Rb.

Given that $g_J = 2$ for both isotopes (equation (2)), $J = \frac{1}{2}$ and $F = I + J = I + \frac{1}{2}$, equation (1) can be rearranged to solve I as a function of g_F:

$$I = \frac{1 - 2g_F \pm \sqrt{g_F^2 + 2g_F + 1}}{2g_F} \tag{9}$$

Using the experimental values for g_F, this can be solved for the nuclear spin of ^{87}Rb:

$$I_{87} = \frac{1 - 2(0.51) + \sqrt{(0.51)^2 + 2(0.51) + 1}}{2(0.51)} \pm 0.07 = 1.46 \pm 0.07$$

And for ^{85}Rb:

$$I_{85} = \frac{1 - 2(0.34) + \sqrt{(0.34)^2 + 2(0.34) + 1}}{2(0.34)} \pm 0.07 = 2.43 \pm 0.07$$

The theoretical values for I are $\frac{3}{2}$ for ^{87}Rb and $\frac{5}{2}$ for ^{85}Rb.[10] Hence, the measured value of I_{87} was 2.7% less than the theoretical value, and the measured value of I_{85} is 2.8% less than the theoretical value.

B. Sweep field calibration

In the following, B is given in Tesla (T) and I is given in amps (A). The table of data for sweep current vs. magnetic field for each isotope is found in Appendix A.

For the ^{87}Rb isotope, the slope of the line of best fit was found to be $\alpha_{87} = (6.17 \pm 0.05) \times 10^{-5}$T/A. For ^{85}Rb, it was $\alpha_{85} = (6.19 \pm 0.05) \times 10^{-5}$T/A. The slope of ^{87}Rb is 0.32% smaller than that of ^{85}Rb, showing that the results are consistent.

For the calibration of the sweep coils in the following experiments, the average of α_{87} and α_{85} was used. This is given by:

$$B_{\text{sweep}} = \alpha_{\text{sweep}} I_{\text{sweep}} \tag{10}$$

where $\alpha_{\text{sweep}} = \frac{1}{2}(\alpha_{87} + \alpha_{85}) = (6.18 \pm 0.04) \times 10^{-5}$T/A

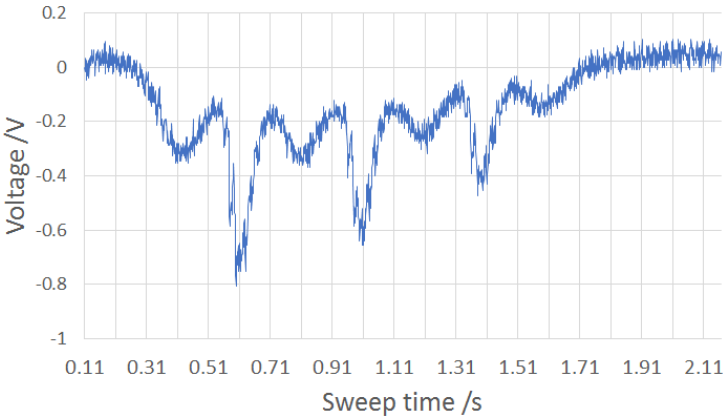

FIG. 4. Quadratic Zeeman effect observed at frequency 5.5Hz

C. Main field calibration

As before, B is given in Tesla (T) and I in amps (A). The table of data for main current vs. magnetic field for each isotope is found in Appendix B.

For ^{87}Rb, the slope of the line of best fit was found to be $\beta_{87} = (5.98 \pm 0.05) \times 10^{-4}$T/A. For ^{85}Rb, it was $\beta_{85} = (1.30 \pm 0.05) \times 10^{-3}$T/A. The slope of ^{87}Rb is 54% smaller than that of ^{85}Rb, which is a very significant difference and one which was not expected. We believe that this discrepancy was due to low fidelity of the detector. At higher frequencies and amplitudes, the noise levels in the results obtained were so large that it was difficult to resolve individual dips, and even harder to measure a dip centre current.

The calibration of the main coils was taken as the average of these two lines, although this does have a large uncertainty due to the large difference between the line gradients. This is given by:

$$B_{\text{main}} = \beta_{\text{main}} I_{\text{main}} \tag{11}$$

where $\beta_{\text{main}} = \frac{1}{2}(\beta_{87} + \beta_{85}) = (9.49 \pm 0.04) \times 10^{-4}$T/A

D. Quadratic Zeeman effect

A plot of the quadratic Zeeman effect occurring at frequency 5.5MHz is shown in FIG. 4.

7 resonances can be observed on this plot, which does not correspond to the expected 6 from ^{87}Rb or 10 from ^{85}Rb. This

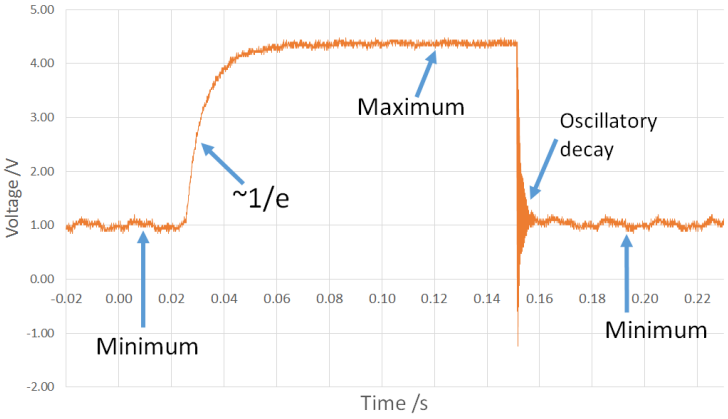

FIG. 5. Example of transient effects, with transmitted light being proportional to the voltage

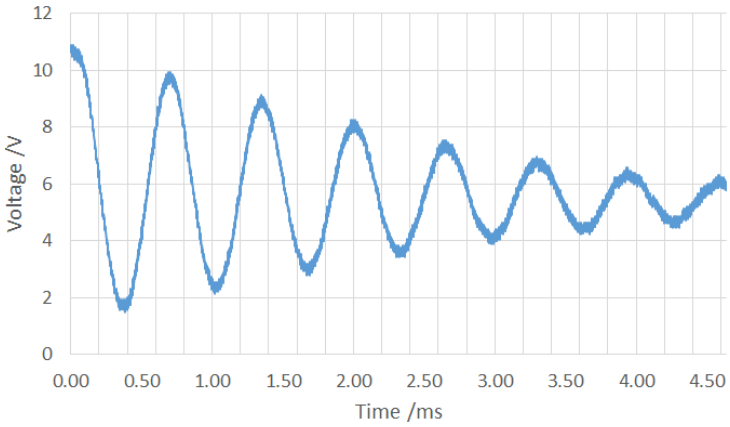

FIG. 6. Close up of transient effect decay

pattern of 7 resonances was also observed at other frequencies and it is not certain as to why. Likely explanations are that the 7^{th} resonance is an artefact of noise, or that our prohibitive noise levels mask the last 3 resonances. It is evident from this graph that the signal received was very noisy, and higher frequencies and RF amplitudes only exacerbated this problem. As a result, measuring the sweep field current for each resonance was not possible as there was no certain point as where this should be measured. Combined with the large uncertainty in the main field calibration (see section V C), this meant that accurately distinguishing the magnetic field at each transmission in the Zeeman effect was unfeasible.

E. Transient effects

FIG. 5 shows an example of the transient effects. The vertical axis shows the voltage through the oscilloscope, which is proportional to the transmitted light through the sample.

The interest of the experiment was in the region where the oscillations of the light intensity occurs. FIG. 6 shows these oscillations close up. It is clear from the figure that these oscillations are sinusoidal and decay with time.

As explored in the experiments section, the time period of these oscillations should be inversely proportional to the applied RF amplitude. FIG. 7 roughly shows the expected inverse relationship. A number of disparate measurements are shown at the smaller amplitude intervals, which is erroneous and likely due to the high noise levels. In fact, the periods

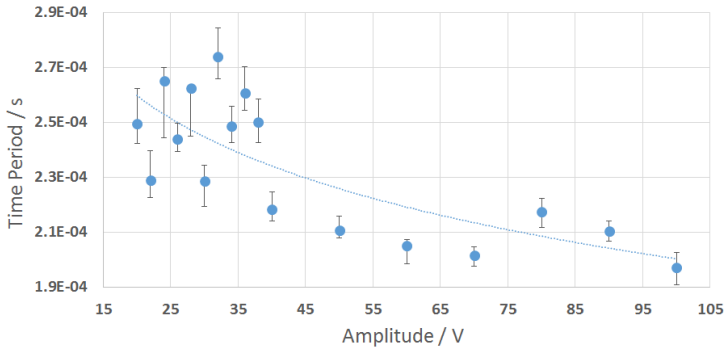

FIG. 7. Transient effect time period, decaying as amplitude increases

of the decaying oscillations from FIG. 6 were seen varying slightly with time on the oscilloscope, verifying that the noise was having a sizeable effect on the observation, rather than some systematic error.

VI. DISCUSSION

In the first set of observations, the experimentally determined values of nuclear spins for ^{87}Rb and ^{85}Rb were both within 3% of the theoretical values, verifying the accuracy of our results. However, most later observations were beset by systematic / random error; our measurements were distorted by astounding noise levels and an almost unexplainable amplitude drift. Minimising or circumventing this noise became imperative for latter measurements. We originally assumed that most of the noise came from external light being picked up by the detector; this "white noise" light would cause the oscilloscope line to become very broad and shaky, meaning any observations we made would be limited in precision by the width of this line.

To combat this, we covered the apparatus to four thick black shrouds, compared to the usual one. This proved worthwhile but insufficient, as the reduced noise levels still exceeded expectation. We then meticulously removed and replaced each cable from the equipment setup and ensured that the banana plugs were in full contact with the input ports. In addition, we moved the apparatus reasonably far away from all nearby metallic objects and realigned it with the Earth's magnetic field. This proved sufficient to reduce the noise to a workable level in most cases, but high precision measurements at high frequencies and amplitudes were still too noisy to be useful.

We concluded that these noise levels must be due to either a unreliable detector or unavoidable proximity to a metallic object e.g. a pipe.

Another source of systematic error was the discrepancy between current amplitude set on the TeachSpin Optical Pumping panel and the actual current amplitude through the equipment. This was trivially resolved by connecting a voltmeter to the panel to record the amplitude. The voltmeter used was digital, eliminating error associated with reading a dial, and had a quantifiable error ± 0.01 V and given a resistance of 1Ω this leads to a current error of ± 0.01 A, which has been included in data plots. It is worth noting that in the calculation of the horizontal magnetic field coils, the resistance corresponding to this voltage measurement was half the size, leading to an error of ± 0.02 V, rather than ± 0.01 V.

VII. CONCLUSION

Our investigation was successful in that we were able to observe several phenomena including hyperfine splitting, drops in intensity originating from the quadratic Zeeman effect and transient effects. Furthermore, our measured Landé g-factors and values of rubidium's nuclear spin were found to be in agreement with the theoretical value. However, the unresolved issues of omnipresent background noise and amplitude drift meant we could not accurately record data and meant the individual amplitudes recorded were not reproducible. These problems particularly impacted upon our investigation into the relationship between the time period of the decaying oscillations caused by transient effects and the applied RF amplitude - though on a macro scale the inversely proportional pattern could be observed regardless of these issues.

VIII. REFERENCES

[1] T. Wolfram, B. Vojak, E. Maas, and R. Burnham, "Optically pumped laser," (1990), US Patent 4,901,330.

[2] T. R. Carver, "Optical pumping," Science **141**, 599–608 (1963), http://science.sciencemag.org/content/141/3581/599.full.pdf.

[3] N. M. AB, "Alfred Kastler - Biographical," `https://www.nobelprize.org/nobel_prizes/physics/laureates/1966/kastler-bio.html` (2014), [Online; accessed 07-02-2017].

[4] TeachSpin, Inc, *Optical Pumping of Rubidium: Student Guide to the Experiment* (2002).

[5] Royal Society of Chemistry, "Rubidium - Element information, properties and uses," (2017), [Online; accessed 08-02-2017].

[6] TeachSpin, Inc., "TeachSpin: Optical Pumping," `http://www.teachspin.com/optical-pumping.html` (2017), [Online; accessed 07-02-2017].

[7] Roderick, J. and Sullivan, .M, "Optical Pumping of Rubidium: Apparatus," `http://spa-mxpweb.spa.umn.edu/s11/Projects/S11_OpticalPumping/apparatus.htm`, [Online; accessed 08-02-2017].

[8] Photonic Detectors, Inc., "PDB-C108," `http://www.datasheetlib.com/datasheet/1247130/pdb-c108_api-advanced-photonix-inc.html` (2017), [Online; accessed 07-02-2017].

[9] Tektronix, "TDS 2024B Digital Storage Oscilloscope," `http://uk.tek.com/oscilloscope/tps2000` (2017), [Online; accessed 07-02-2017].

[10] S. Millman and M. Fox, "Nuclear Spins and Magnetic Moments of Rb^{85} and Rb^{87}," Phys. Rev. **50**, 220–225 (1936).

Appendix A: Sweep field calibration data

TABLE I. Sweep calibration- Rubidium-87

Sweep current /A	Magnetic field ± 0.05 /10^{-5}T
0.324	1.99
0.352	2.13
0.376	2.27
0.397	2.42
0.424	2.56
0.446	2.70
0.466	2.85
0.489	2.99
0.512	3.13
0.536	3.27
0.560	3.42
0.580	3.56
0.599	3.70
0.723	4.42
0.837	5.13
0.955	5.85

TABLE II. Sweep calibration- Rubidium-85

Sweep current /A	Magnetic field ± 0.05 /10^{-5}T
0.359	6.43
0.397	8.57
0.431	1.07
0.468	1.29
0.500	1.50
0.536	1.71
0.571	1.93
0.606	2.14
0.639	2.36
0.674	2.57
0.707	2.79
0.744	3.00
0.769	3.22
0.954	4.29

Appendix B: Main field calibration data

TABLE III. Main calibration- Rubidium-87

Main current /A	Magnetic field ± 0.05 /10^{-4}T
0.047	4.11
0.099	5.31
0.160	7.11
0.187	9.04
0.161	1.06
0.185	1.21
0.237	1.47
0.297	1.84
0.358	2.20
0.482	2.92
0.726	4.35
0.972	5.78

TABLE IV. Main calibration- Rubidium-85

Main current /A	Magnetic field ± 0.05 /10^{-4}T
0.047	1.12
0.099	1.46
0.160	1.64
0.187	1.83
0.161	1.99
0.173	2.25
0.203	2.70
0.245	3.23
0.286	3.76
0.368	4.84
0.532	6.99
0.698	9.12